POLITECNICO
MILANO 1863

SCUOLA DI INGEGNERIA INDUSTRIALE
E DELL'INFORMAZIONE

Executive Summary of the Thesis

$La_{2-x}Sr_xCuO_4$ thin films and nanostructures to study local ordering phenomena in a striped superconductor

Laurea Magistrale in Engineering Physics - Ingegneria Fisica

Author: Marco Biagi

Advisor: Prof. Giacomo Claudio Ghiringhelli

Co-advisor: Dr. Riccardo Arpaia, Prof. Alexei Kalaboukhov

Academic year: 2021-2022

1. Introduction

Since their discovery in 1986, cuprates high critical temperature superconductors (HTS) represent the preeminent challenge in condensed matter physics. Understanding the underlying mechanism behind high-T_c superconductivity is a real challenge, which could results in the possibility to design in the future a room-temperature superconductor, a technological holy grail allowing an energy-efficiency revolution, and the large-scale realization of applications such as magnetically levitated trains and quantum computers. The strong electron-electron correlations in this class of compounds lead to the formation of exotic charge and spin orders such as charge density waves (CDW) and spin density waves (SDW), that are respectively charge and spin density periodic spatial modulations. In La-based cuprates, as $La_{2-x}Sr_xCuO_4$ (LSCO), they are characterized by a well defined relation of periodicity, forming the so-called stripe order, but long-ranged CDW, without spin-charge locking, and short-ranged charge density fluctuations (CDF) are also present, therefore showing to be ubiquitous in all cuprate families. Although static stripes compete with superconductivity, it has been proposed that CDF may be pivotal to understand the anomalous properties of both the normal and superconducting state. The nature of these nanoscale orders can be effectively investigated in thin films, where the strain induced by the substrate, and the confinement due to nanostructures of reduced dimensions, have proven to be two powerful knobs to manipulate these orders and understand their mutual interaction. The fabrication of HTS nanostructures is a very challenging task, and up to now relevant results were obtained mainly for $YBa_2Cu_3O_{7-\delta}$ (YBCO). We optimize the growth of 15 u.c. optimally doped LSCO thin films, considered a model system for cuprates, on $LaSrAlO_4$ (001) substrate by pulsed laser deposition. The surface morphology of the films was characterized with Reflection High Energy Electron Diffraction (RHEED) and Atomic Force Microscopy (AFM), while the structural quality of the film was evaluated by X-ray diffraction (XRD), and X-ray Reflectivity (XRR). The transport properties were measured with a Physical Property Measurement System (PPMS), from room temperature down to T = 5 K. Some of the samples were post-annealed in an ozone-rich environment to study the effect of excess oxygen. Moreover, we fabricate

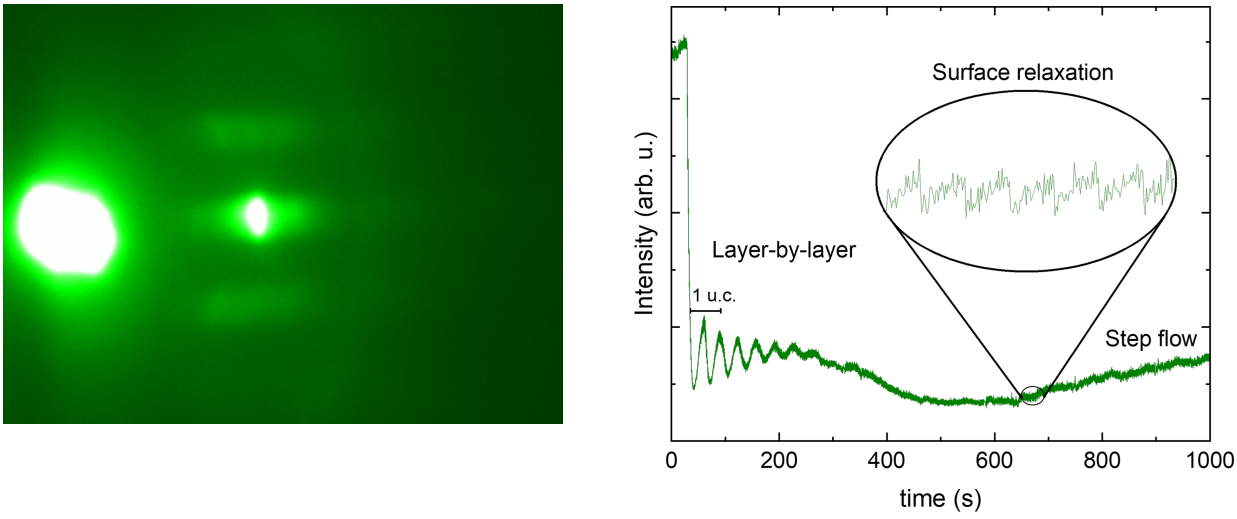

(a) (b)

Figure 1: a) RHEED pattern of one representative LSCO film after the deposition, b) intensity as a function of time of the central spot of the RHEED pattern during the growth. The oscillations during the first part of the growth are characteristic of the layer-by-layer growth (LBL). Then, the growth mode changes to step flow (SF). The signal is magnified in the inset to highlight the surface relaxation characteristic of the layer-by-layer and step flow growth mode.

nanowires of width down to 50 nm. We extracted the value of the critical current density J_c from the current-voltage characteristic (IVC), and we studied the J_c temperature dependence of the narrowest nanowire from 4.2 K up to the critical temperature. J_c is extremely sensitive to any inhomogeneity in the superconducting properties along the bridge [1], hence to confirm the quality of our superconducting bridges we compared the values of J_c with the theoretically expected Ginzburg-Landau (GL) depairing limit, valid for bridges with cross sections smaller than the London penetration depth λ_L.

2. Film growth and characterization

$La_{1.85}Sr_{0.15}CuO_4$ ultra-thin films were grown on $LaSrAlO_4$ (LSAO) (001) by PLD using an KrF excimer laser ($\lambda = 248$ nm). LSAO is isostructural with LSCO, but with an in-plane lattice constant $a_{LSAO} = 3.756$ Å, that is 0.5% smaller than LSCO ($a_{LSCO} = 3.777$ Å). Therefore, LSAO induce an in-plane compressive strain on the LSCO film. This causes the elongation of the c axis and tend to increase the T_c of the films [2]. The temperature during the deposition (T_{dep}) and the oxygen partial pressure (P_{dep}) were set to 750 °C and 0.1 mbar respectively. The laser energy (E), and the spot size of the laser (A_{spot}) impinging on the target, together with the target-substrate distance (d_{TS}), were kept as free parameters for the optimization of the growth conditions. All film thicknesses are set constant at 200 Å, except for one sample of 500 Å used for the nanowires fabrication.

In figure 1a the in-situ RHEED pattern of a representative LSCO film after the growth is shown. The presence of one intense spot is the indication of a 2D surface. However, the slightly streak-like elongation of the peaks may indicate a marginal presence of small crystal domains on the surface. In figure 1b the intensity of the RHEED pattern monitored during the growth is reported. From the oscillations in the first part of the growth, characteristic of layer-by-layer (LBL) growth, it has been possible to retrieve the grow rate of the film, and estimate the deposition time for 15 unit cells (20 nm). The growth mode eventually changes to step flow (SF) as demonstrated by the surface relaxation at each laser pulse (inset of figure 1b).

In figure 2 the image of the surface of one representative sample is shown. The average surface roughness (R_q) is small ($\sim$ 0.6 nm). However, one can notice the presence of precipitates of width $\sim$ 50 nm on the surface, indicating an excess of some of the constituent elements of the

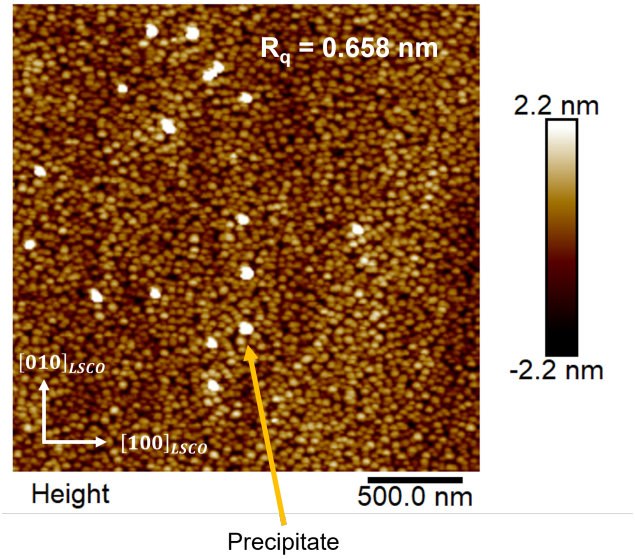

Figure 2: AFM image of the surface of one of the films after the deposition. Despite the presence of precipitates (indicated by the arrow) on the film, the surface is flat with a low roughness value R_q. The image was taken in tapping mode.

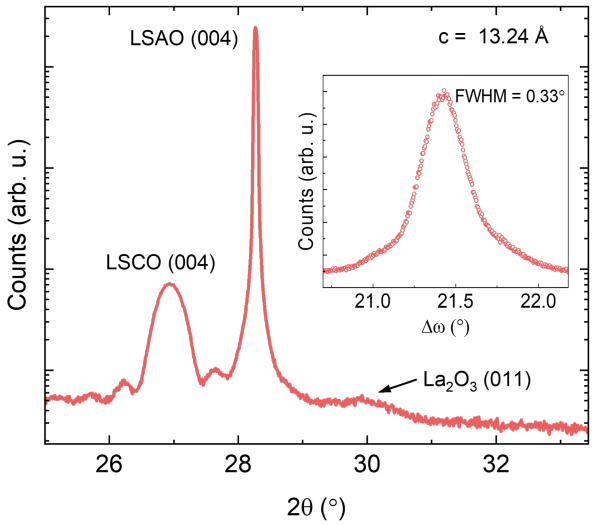

Figure 3: $2\theta - \omega$ symmetric scan of the LSCO (004) and LSAO (004) reflections. It is possible to note the presence of a smaller extra peak, corresponding to the La_2O_3 (011) reflection. The out-of-plane c parameter, estimated from a $2\theta - \omega$ scan in the range 10°-80° (not shown) is reported in the top right part of the plot. In the inset the rocking curve of the LSCO 006 reflection in reported, together with the value of its FWHM.

film, that contribute to increase R_q.
The film thickness was confirmed by specular XRR measurements (not shown), for which we found a value of $t \sim 18.5$ nm. The small mismatch (about 1 u.c.) between these value and the expected one is due to a possible change of the growth rate when the growth mode changes from LBL to SF. The quality of the crystal structure of the film was instead investigated by XRD measurements. In figure 3 a symmetric $2\theta - \omega$ scan around LSCO (004) reflection is presented. From the position of this peak, together with those of the other (00n) peaks in the range 10°-80° (not shown) it has been possible to estimate the out-of-plane lattice parameter $c = 13.24$ Å, confirming that the film is actually under compressive strain (in the bulk $c_{LSCO} = 13.226$ Å). Moreover, it is possible to note the presence of a small peak corresponding to the La_2O_3 (011) reflection. We have associated the presence of this peak with the presence of precipitates on the surface observed with the AFM (see figure 2). The inset of figure 3 shows the rocking curve (RC) of the LSCO (006) reflection. Although sharp, the RC peak is broader than in other LSCO films reported in literature with similar thickness [3]. This broadening could be due to the presence of the precipitates in the film, that may induce a higher degree of disorder.

The transport properties of the films were measured in Van der Pauw geometry, bonded with aluminum wire. Silver paint was placed on the bonds to reduce the contact resistance. In figure 4 the R(T) normalized at its value at 45 K is shown for one of our best film in the temperature range around the superconducting transition, together with its first derivative. The T_c^{on} is about 38 K, and the T_c^0 is around 25 K. Our results are comparable with the reference values for the bulk compound, where $T_c^{on} \approx 39$ K and $T_c^{mid} \approx 37$ K. However, our transition is broader with respect to the bulk one. The same broadening has been already reported in literature [3]. It can be due to the presence of oxygen vacancies, or to the higher degree of disorder of the film under strain with respect to the bulk. In particular, comparing our results with previous work, for films of similar thickness (10 nm), and where the stoichiometry of the film has been confirmed by Rutherford backscattering, very similar values of $T_c^{on} \approx 40$ K and $T_c^0 \approx 25$ K for optimally doped LSCO films were reported [3].
In general we have obtained a spread of the T_c values for our films. This is a well know problem in LSCO films also grown by MBE. Naito at al. [4] have underlined the crucial importance of

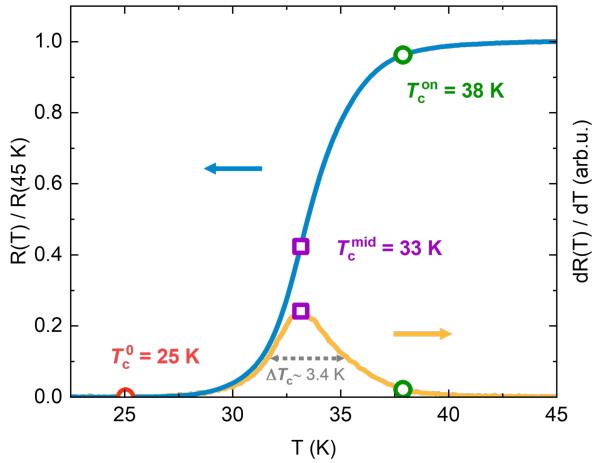

Figure 4: In-plane R(T) normalized at 45 K, and dR(T)/dT around the superconducting transition for one of the best obtained film. The onset of the transition, defined as the 10% of the first derivative is reported in green. In purple the midpoint of the transition, defined as the maximum of the first derivative. In red the T_c^0, defined as the temperature at which the resistance completely vanish. The width of the transition is reported in gray, defined as the FWHM of the first derivative. The width of the superconducting transition is defined as the FWHM of the first derivative.

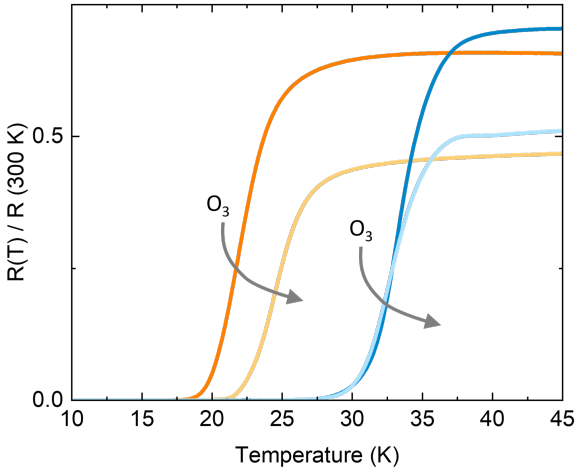

Figure 5: Effect of the ozone post-annealing on two samples. The R(T) are normalized on the R(T = 300 K) value for an easier comparison of the results. The orange line is one sample representative for the "low T_c" films before the post-annealing in ozone, while the yellow line is the same sample after the post-annealing. The blue and light-blue lines belong to the best sample with highest T_c before and after the post-annealing in ozone.

the substrate surface quality for the growth of LSCO film. Indeed, they obtained a large spread of the T_c values of LSCO films grown on untreated LSAO, and they managed to reduce this spread after chemical etching of the LSAO substrate with a methanol solution of hydrocloric acid (HCl). We have tried to repeat that process for our samples, but unsuccessfully. On the contrary, the chemical etching has considerably deteriorated the surface of the substrate. The reason of the difference between our result and that of ref. [4], concerning the chemical etching process, is still under investigation. To further confirm the stoichiometry of our sample with the highest T_c, we have studied the effect of ozone post-annealing. Indeed, it is well known that in underdoped LSCO the T_c is very sensitive to the oxygen content, while in optimally doped LSCO the change in T_c due to extra oxygen is negligible [2]. We have post-annealed some films with lower critical temperature and one of the best film with higher critical temperature in an O_3/O_2 mixture. The results are summarised in figure 5. In the case of the film with lower T_c the critical temperature changed considerably, while in the film with higher T_c the effect of the annealing was negligible. This, together with the comparison of the T_c values with reference where the stoichiometry was confirmed by Rutherford backscattering [3], bring to the conclusion that our films with the highest T_c are actually optimally doped LSCO films.

3. Nanowires fabrication

To define the nanowires, we have used a 100 nm thick amorphous carbon layer as hard mask, in combination with electron beam lithography at 100 kV, and Ar^+ ion etching. The etching step is the most crucial. The interaction of Ar^+ ions

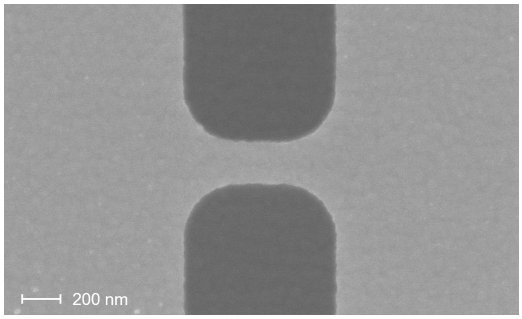

Figure 6: SEM image of one 200 nm width wire. It can be notice the nanowire geometry design in order to avoid current crowding effects at the corner between the bridge and the electrodes.

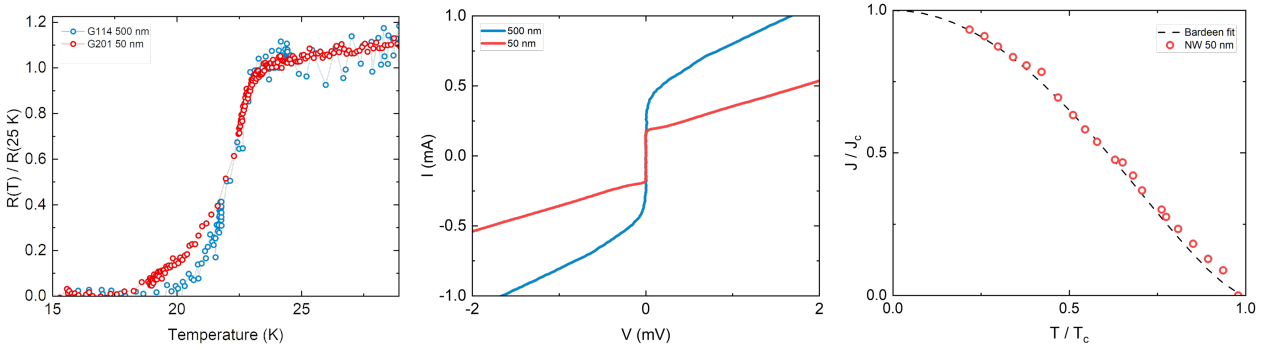

(a) (b) (c)

Figure 7: Measurements of a) the resistance versus temperature normalized at R(25 K) and b) the current voltage characteristic for a 50 and a 500 nm width nanowire. Bardeen fit of the temperature dependence of the critical current density c), from 4.2 K up to the transition temperature, for a 50 nm width nanowire. The data are normalized on the critical current density at zero temperature J_c^0 and the critical temperature T_c.

with the LSCO may cause severe degradation of the transport properties due to changes in the film stoichiometry and disorder. For this reason, we have decided to operate at low voltage ($\sim$ 300 V), and we have calibrated carefully the etching time to minimize the interaction of Ar^+ ions with the nanostructures. The dimensions of the nanowires were verified before the etching step with SEM (shown in figure 6). Moreover, to increase the quality and reproduciblity of the results, the film was capped with a 50 nm thick Au layer before the hard C mask deposition. It is demonstrated that the Au capping layer is fundamental to obtain high quality nanostructures. Indeed, it mitigates the overheating of the superconducting bridges during the Ar^+ ion milling, and protects their surface during the O_2 plasma etching needed to remove the C mask at the end of the fabrication [5]. It is worth mentioning that the geometry of the nanowires has been designed in order to reduce current crowding effects. Indeed, in case of sharp angles between the bridge and the electrodes, the current density at the inner corners is enhanced compared to the average current density at the centre of the bridge. This causes the current density at the corner to reach the critical values while in the centre of the wire it is still below that limit. As a consequence, the average critical current density of the nanowire is reduced, even for bridges whose width is smaller than the Pearl length $\lambda_P = \lambda^2/t$.

4. Nanowires measurements

We realized nanowires of different widths, from 500 nm down to 50 nm. We have measured 107 nanowires in total. For each nanowire the current voltage characteristic (IVC) was carried out, while the resistance and critical current density temperature dependence were studied only for a restricted number of devices. In figure 7a) the normalized R(T) around T_c for a 50 and a 500 nm width wires is reported. The narrowest bridge transition is broader than the wider one due to thermal fluctuations. Indeed, the energy barrier for the Abrikosov vortices crossing the bridge is proportional to the width of the wire. In figure 7b) the IVC at 4.2 K for a 50 and a 500 nm wide wire is reported. The IVC for the wider wire is flux-flow like in the entire range of voltage bias. Instead, the 50 nm wire present a small switch from zero voltage to a finite voltage state at lower bias: the reason is still under investigation, but this is in agreement with previous result obtained for YBCO nanowire having the same width [5]. From the IVC it has been possible to extract the value of J_c using a voltage criterion of 20 μV. We obtained an average value of $J_c^{50} = 6.9 \times 10^6$ A/cm^2 for the 50 nm width nanowires, and an average value of $J_c^{500} = 1.1 \times 10^6$ A/cm^2. Since reducing the dimensions of the wire it is possible to approach the GL depairing limit it is reasonable that we obtained a higher J_c for the narrowest bridges. Finally, in figure 7c) the $J_c(T)$ for a 50 nm width nanowire is presented. The data are well fitted

by the Bardeen expression:

$$J_c(T) \propto J_c^0 \left[1 - \left(\frac{T}{T_c}\right)^2\right]^{\frac{3}{2}} \quad (1)$$

from which it has been possible to retrieve the $T_c = 23.5$ K, and the value of the critical current density as zero temperature $J_c^0 = 7.7 \times 10^6$ A/cm^2. This J_c^0 value has to be compared with the GL theoretical limit for the depairing current due to vortex entry:

$$J_v = 0.826 \frac{\phi_0}{3\sqrt{3}\pi\mu_0\lambda^2\xi} \quad (2)$$

where λ is the London penetration depth, ξ the coherence length, ϕ_0 the magnetic flux quantum, and μ_0 the vacuum permeability. Values of $\lambda = 500$ nm and $\xi = 3$ nm were used to calculate the expected deparing current compatible with $T_c = 23.5$ K, giving $J_v = 1.2 \times 10^7$ A/cm^2. The J_c^0 of our nanowires is close (by a factor of ~ 1.5) to the theoretical GL limit. This is a strong indication of the quality of our nanowires, in terms of uniformity of the transport properties. The high homogeneity of the wires is further confirmed the Bardeen-like $J_c(T)$, that has been observed only in defect-free YBCO nanowires [1]. The little discrepancy between our value of J_c^0 and the GL J_v may be due to the non-optimal quality of the film used for the fabrication, or to impurities introduced during the nanowire fabrication. However, the results obtained for the nanowires point towards the former scenario.

5. Conclusions

We successfully optimized the growth of optimally doped LSCO thin films (15 u.c.) by PLD, with T_c comparable to the one of the bulk. The spread of T_c in our film is probably due to the surface quality of the substrate. Moreover, we successfully fabricate LSCO nanowires down to 50 nm width, and verified their remarkable quality measuring the $J_c(T)$, and comparing our results with the expected ones. There are no previous work reporting LSCO nanowires with dimensions and quality comparable to ours.
We propose two ways to reduce the spread of the T_c of our films for future studies, that probably will also improve the quality of the films, allowing to obtain extremely homogeneous nanostructures: 1) growing LSCO film on STO with a LSAO buffer layer, such as to investigate the effect of the surface quality on the T_c. 2) Annealing the LSAO substrate in a La-rich environment to obtain single-terminated surface.
Our results are encouraging for the growth of underdoped LSCO and the fabrication of state-of-the-art nanowires to study how and if the nanoscale orders are modified by strain in LSCO.

6. Acknowledgements

I want to thank my supervisor Prof. Giacomo Ghiringhelli, for the opportunity he gave me, and my co-advisors Prof. Alexei Kalaboukhov, and Dr. Riccardo Arpaia, for all the stimulating discussions and all the help they gave me both inside and outside the cleanroom.

References

[1] S. Nawaz *et al.*, "Approaching the theoretical depairing current in $YBa_2Cu_3O_{7-x}$ nanowires," *Physica C: Superconductivity*, vol. 495, pp. 33–38, 2013.

[2] I. Bozovic *et al.*, "Epitaxial Strain and Superconductivity in $La_{2-x}Sr_xCuO_4$ Thin Films," *Phys. Rev. Lett.*, vol. 89, no. 10, p. 107001, 2002.

[3] S. Das *et al.*, "Structural, magnetic, and superconducting properties of pulsed-laser-deposition-grown $La_{1.85}Sr_{0.15}CuO_4/La_{2/3}Ca_{1/3}MnO_3$ superlattices on (001)-oriented $LaSrAlO_4$ substrates," *Phys. Rev. B*, vol. 89, no. 9, p. 094511, 2014.

[4] M. Naito *et al.*, "Epitaxial effects in thin films of high-T_c cuprates with the K_2NiF_4 structure," *Physica C: Supercond. Appl.*, vol. 546, pp. 84–114, 2018.

[5] R. Arpaia *et al.*, "Improved Nanopatterning for YBCO Nanowires Approaching the Depairing Current," *IEEE Trans. Appl. Supercond.*, vol. 23, no. 3, pp. 1101505–1101505, 2013.